Resonant Rayleigh scattering by excitonic states laterally confined in the interface roughness of GaAs/Al_xGa_{1-x}As single quantum wells

N. Garro, L. Pugh, R. T. Phillips, V. Drouot, M. Y. Simmons, B. Kardynal, and D. A. Ritchie
Cavendish Laboratory, Madingley Road, Cambridge CB3 0HE, United Kingdom
(Received 31 January 1997)

A systematic study of resonant Rayleigh scattering (RRS) in semiconductor single quantum wells (QW's) is reported. The QW's were grown under different conditions leading to different interface roughness. High spatial and spectral resolution photoluminescence (PL) and PL-excitation (PLE) measurements revealed that the electronic configuration of the wells is very sensitive to the growth conditions. RRS and multichannel PLE, which can be related to the absorption, were measured simultaneously in order to study the redshift of the RRS with respect to the absorption. The dependence of this shift on the full width half maxima of the transitions studied showed remarkable differences depending on the interface roughness profile. RRS intensity was found to be very sensitive to the inhomogeneous broadening of the transitions. The temperature dependence of RRS from 1.4 to 40 K is also reported. The decrease in the intensity and in the redshift between RRS and PLE found in the experiment when temperature is raised can be explained in terms of thermal detrapping of laterally confined excitons. [S0163-1829(97)05420-9]

I. INTRODUCTION

In 1982, Hegarty *et al.*[1] reported for the first time a resonant enhancement of the Rayleigh scattering at the heavy-hole (hh) exciton transitions of GaAs/Al_xGa_{1-x}As multiple quantum well structures. Spatial fluctuations in the well width that cause spatial fluctuations in the refractive index were identified as the origin of the elastic scattering of light in the whole solid angle (Rayleigh scattering). Hegarty *et al.* presented a macroscopic theoretical treatment of the process that gave relative values for the homogeneous broadening (Γ) usually obscured by the inhomogeneous broadening (Λ) in this kind of system.[1,2] Thus resonant Rayleigh scattering (RRS) appeared as a powerful technique for the study of the dynamics of excitons in quantum wells (QW's) capable of use at very low excitation intensities where other methods such as hole burning or photon echoes present problems. Despite these advantages, the use of RRS was inexplicably abandoned for almost a decade. The experimental progress in time resolution in the early 1990s allowed the development of time-resolved light-scattering spectroscopies[3] and, in particular, time-resolved RRS. According to the theoretical predictions of Stolz and coworkers[3–5] the RRS signal, even for complex inhomogeneously broadened systems, decays with the intrinsic coherence time of the excitonic states T_2, related to Γ by $\Gamma=\hbar/T_2$.

Despite the relevance of the results obtained with RRS in the study of QW systems, almost no attention was paid to the RRS process itself. It was only recently that the first experimental[6,7] and theoretical[8–10] attempts were made at a microscopic description of the process. Discussion has been centered on the nature of the intermediate excitonic states participating in the scattering. As a consequence of wave-vector conservation, confined excitonic states give the main contribution to the scattering efficiency[8] in systems with small disorder such as crystalline solids. In semiconductor QW's excitons are confined (or localized) by two-dimensional (2D) growth islands formed at the well interfaces during the growth process. Formally all the excitonic states may be localized, however, for practical purposes, those with sufficiently large localization length may be considered ''propagating'' or delocalized states. Confined states correspond to slightly lower energies than propagating states and thus correspond to the low-energy side of the absorption peak. The redshift of the RRS with respect to the photoluminescence excitation (PLE) found for the hh transition in QW systems[1,6,7] was then taken to be a consequence of the presence of localized states and therefore as a general feature of real QW structures.[6]

The optical response of semiconductor QW's is very much dependent on the growth conditions through the quality of the interfaces. Well width fluctuations are unavoidable and lead to inhomogeneous broadening of the optical transitions. However, recent investigation in growth techniques[11,12] have proved that the control of the growth temperature and the time the growth is interrupted at the interface can lead to bigger and more separated growth islands. Spatially resolved PL measurements on those kinds of samples have resulted in very sharp peaks (linewidths down to ≈ 40 μeV, see Gammon *et al.*[13]) that show the single-exciton character of the transitions.[13–15]

In this paper we present a systematic study of RRS in semiconductor single QW's with the aim of throwing light on the nature of this process. We analyze carefully the scattering process with the help of a microscopic picture in order to determine the localized or extended nature of the excitonic states participating in the scattering. High-resolution RRS measurements at the hh exciton transitions in different sized QW's (from 40 to 200 Å) were undertaken in order to address the RRS dependence on the inhomogeneous broadening of the transition. Experimental evidence about the character of the intermediate states, either confined or propagating, was gathered by investigating two samples with very different excitation pictures due to differences in the

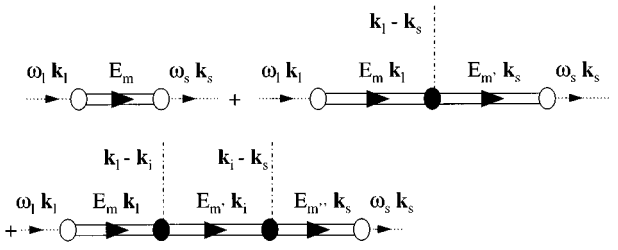

FIG. 1. Feynman diagrams contributing to the Rayleigh scattering amplitude. Dotted lines represent incoming and dispersed photons, double lines correspond to intermediate excitonic states, and the dashed lines represent impurities of the perfect lattice.

typical length scale of their interface roughness. If confined states give the main contribution to RRS, one should expect a high dependence of the scattering efficiency on temperature as a consequence of the temperature dependence of state lifetimes through scattering by acoustic phonons. The temperature dependence of the RRS is regarded for temperatures from 1.4 to 40 K, for QW's of several widths and also for bulk GaAs.

This paper is organized as follows. A theoretical description of the Rayleigh scattering process is given in Sec. II. In Sec. III the two samples studied in this work are described, emphasizing that the differences in the growth conditions have caused important differences in their exciton spectra. Details about the experimental setup are given in the end of that section. The redshift of the RRS with respect to the absorption spectrum is analyzed for both types of sample and for several well widths, and also for the bulk in Sec. IV. In Sec. V RRS intensity and line shape are analyzed in terms of the homogeneous and inhomogeneous broadening of the transition. Section VI deals with the variation of the RRS profile with temperature. And, finally, Sec. VII summarizes the main conclusions of the work.

II. THEORETICAL BACKGROUND

In a RRS process the incoming light is elastically dispersed in the whole solid angle and the resonance occurs when the excitation energy is equal to the energy of a real excited state of the system. This process is microscopically analyzed in this section. A diagrammatic picture of the process is very useful in understanding the nature of the process. Some lower-order Feynman diagrams contributing to RRS are depicted in Fig. 1. The first diagram in Fig. 1 represents the absorption of a photon $(\omega_l, \mathbf{k}_l)$ by the solid with the creation of an exciton in the state m; in the second step the exciton is destroyed with the emission of a photon $(\omega_s = \omega_l, \mathbf{k}_s)$. In the following diagrams the photoexcited exciton interacts elastically (only wave vector is transferred in the scattering) with one or more static defects of the solid. This interaction is represented by the full vertex. The contribution of the excitonic propagators (double lines in Fig. 1) to the scattering amplitude is proportional to

$$\sum_m \frac{1}{E_m - \hbar\omega_l + i\Gamma_m/2} e^{i(\mathbf{k}_s - \mathbf{k}_l)\mathbf{r}_m}, \qquad (1)$$

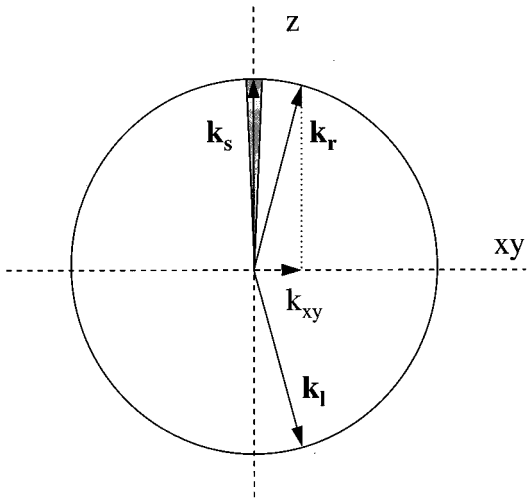

FIG. 2. Plane section of the phase sphere for a RRS process for Brewster's angle scattering geometry. $\mathbf{k}_l$, $\mathbf{k}_r$, and $\mathbf{k}_s$ are the incident, reflected, and scattered photons, respectively. The shaded area corresponds to the collection cone.

where E_m, Γ_m, and $\mathbf{r}_m$ are the energy, the homogeneous broadening, and the position vector of the state m. Equation (1) explains why the scattering is resonant when $\hbar\omega_l \approx E_m$.

The microscopic picture also helps to clarify the selection rules of the process and especially the controversial issue of the character of intermediate states.[6–8] Let us analyze first the lowest-order diagram of Fig. 1. If the intermediate states are ideal propagating states, then the wave-vector conservation principle fixes the scattering direction $(\mathbf{k}_s = \mathbf{k}_l)$ and only forward scattering is possible. For confined states, on the other hand, the wave-vectors are not good quantum numbers and their conservation is relaxed. In lowest-order perturbation theory only confined excitonic states contribute to RRS. In higher-order terms, the participation of static defects removes any constraint on the character of the intermediate states and both confined and propagating states contribute to the scattering efficiency. In QW systems, where fluctuations in the well width have led to lateral confinement of the exciton center of mass wave functions, RRS comes mainly from the first diagram in Fig. 1, i.e., from confined intermediate states.

It is helpful to make the description given in the previous paragraph more quantitative with regard to the degree of confinement of the lateral wave function that this model of RRS demands. In real QW systems all excitonic states are formally localized due to fluctuations in the well width and even those considered to be propagating states have a finite diffusion length[16] because the finite exciton lifetime. To determine the level of confinement required in the lowest-order RRS process one has to analyze carefully the wave-vector change that occurred in the process. Figure 2 shows the scattering geometry corresponding to incidence near to Brewster's angle $(\theta_B \approx 75°)$ and collection in an $f/3$ cone around the growth axis (z). The high refractive index of GaAs implies only a small angle ($\approx$ from 12° to 20°) between the incident and the scattered wave vectors. Energy conservation implies

$$|\mathbf{k}_s| = |\mathbf{k}_l| = n\frac{2\pi}{\lambda}, \tag{2}$$

where n is the refractive index and λ the wavelength of the incident light. Confinement of the center of mass wave function in the plane of the well relaxes the conservation of the wave vector in that plane. The same effect for the confinement in the growth direction permits final states contributing to scattering in the collection cone to satisfy overall conservation of $|\mathbf{k}|$ required by energy conservation. In order to scatter into the collection cone, the in-plane wave-vector uncertainty has to be relaxed to at least the extent of

$$\Delta k_{xy} \approx \frac{2\pi}{\lambda}\sin\theta_B . \tag{3}$$

Therefore any exciton localized on a length scale smaller than

$$\Delta \ell_{xy} \leqslant \frac{\lambda}{\sin\theta_B} \tag{4}$$

will contribute to the RRS process described by the first diagram of Fig. 1. Excitons localized on a length scale larger than this are those we consider to be propagating states for the purposes of RRS. For an incident wavelength of 8000 Å $\Delta \ell_{xy} \leqslant 0.83$ μm. The confinement required for Brewster angle scattering geometry is not very severe.

III. SAMPLE DESCRIPTION AND EXPERIMENTAL SETUP

A. Samples growth

The two samples investigated in this work were grown on GaAs [001]-oriented substrates in two different MBE machines; one of the samples, the one that will be referred to as sample *A* from now on, was grown in a Varian Gen II and the other one, sample *B*, in a Vacuum Generator V80H MBE machine. Both samples consist of GaAs single QW's of several widths (from 20 to 300 Å) separated by 150-Å $Al_{0.33}Ga_{0.66}As$ barriers. Sample *A* was indium mounted on a molybdenum block for growth and sample *B* held in an indium-mounting free block. Nominally, growth conditions were comparable in terms of growth rates and arsenic overpressure, however, sample *A* was grown continuously at a substrate temperature of 650 °C whereas sample *B* was grown at a lower substrate temperature of 570 °C and, more importantly, the growth was interrupted for 2 min and 5 s at each heterointerface. In both cases substrate temperatures were measured using an optical pyrometer. For the growth interrupts used in sample *B* the arsenic flux was kept on for the first minute, closed for 5 s and then turned on for the last minute. Scanning tunneling microscope studies of growth-interrupted GaAs surfaces have revealed large two-dimensional islands of typical size larger than the exciton Bohr radius[15] (a_B).

B. Optical characterization

Both samples were characterized using standard optical techniques: PL and PLE spectra were recorded for the hh exciton at the different wells. The PLE spectrum is conventionally obtained by integrating the luminescence at a single wavelength, which is usually chosen at the low-energy side of the PL peak. Under ideal conditions, when the nonradiative recombination is negligible and the relaxation is much faster than the radiative recombination, the PLE spectrum can be assumed to be equivalent to absorption. Nevertheless, due to the lateral confinement of excitons in the interface roughness, conventional single-channel PLE is extraordinarily dependent on the final state and on the relaxation process and therefore cannot be related to the absorption.[17] This problem can be reduced by extending the integration to the whole luminescence peak so that all the most important emission channels are being considered. Assuming that all the absorbed light is reemitted, which is valid for good quality QW systems, then this *multichannel* PLE is proportional to the absorption spectrum. Remarkable differences are found between the two samples. Both samples show a redshift of the PL peak with respect to absorption, but while it increases considerably in sample *A* as the wells become narrower (the measured splittings go from 0.02 meV for the 300-Å QW to 5.2 meV in the 40-Å well) in sample *B* this shift is always very small (it is only 0.15 meV for the 56-Å QW). In sample *A* the redshift between the two spectra (Stokes' shift) is comparable to the broadening of the PL peak, whereas in sample *B* it is much smaller than the measured full width at half maximum (FWHM)—there is a difference of one order of magnitude. The variation with the well width of the Stokes shift between the PL and the absorption is shown in Fig. 3. Also the FWHM exhibit dissimilarities: in sample *A* the absorption peaks are wider than the PL ones, as is usually found; in sample *B*, on the other hand, both spectra show similar linewidths for all the transitions studied.

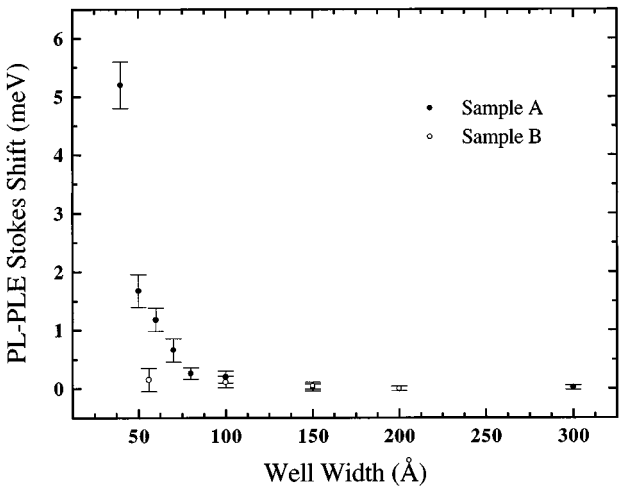

FIG. 3. Stokes shift between PL and multichannel PLE as a function of the well width in the two samples studied.

The unusual behavior of sample *B* was studied further by the use of a sampling method that restricted the probed area to squares $\leqslant 1$ μm^2. This method consists of covering the sample with a thin film of Al (100 nm), which is opaque to typical $GaAs/Al_xGa_{1-x}As$ transition wavelengths. Electron-beam lithography is used to produce a series of apertures of diameter varying from 5 down to 0.5 μm. Figure 4 shows the PL spectrum of the hh exciton for the 28-Å QW measured

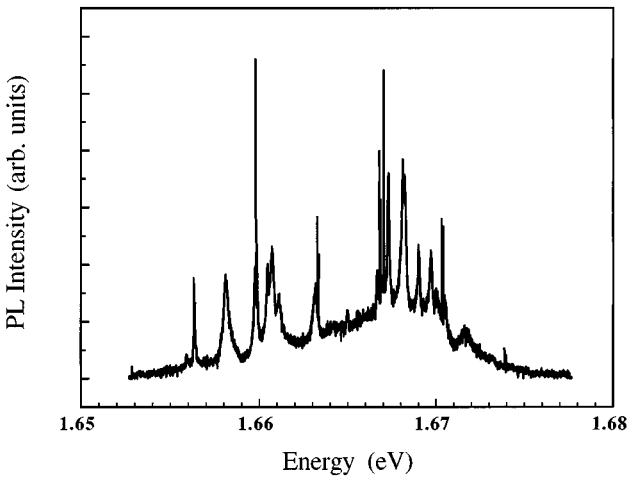

FIG. 4. PL spectrum for the 28-Å QW in sample *B* measured through an aperture of 0.6 μm of diameter. The laser power employed in the experiment was of 300 μW/mm^2 and the temperature was of 4.2 K (this temperature was measured at the He exchange area of the cryostat).

through an aperture of 0.6-μm diameter. The PL profile is formed by a large number of very sharp peaks (undeconvolved FWHM of 60–100 μeV) irregularly separated in energy. By standard macroscopic PL techniques it is only possible to obtain laser spots down to 50 μm diameter. With the use of the aluminum masking we found that for areas smaller than 1 μm^2 the inhomogeneities are spectrally resolved. The resolution of these measurements was limited by the spectrometer and was 30 μeV. Single-channel standard PLE was also performed on sample *B*. Figure 5 shows PLE spectra corresponding to the hh exciton transition of the 28-Å QW through a 1-μm-diam aperture. The spectrometer was set at different positions of the low-energy side of the emission (the detection energies are shown by arrows). The PLE spectrum is extremely dependent on the detection energy due to the isolation of the different growth islands. PLE shows only those excited states that couple to the detected quantum dot transition, and cannot be simply proportional to absorption, as has been pointed out earlier in this section.

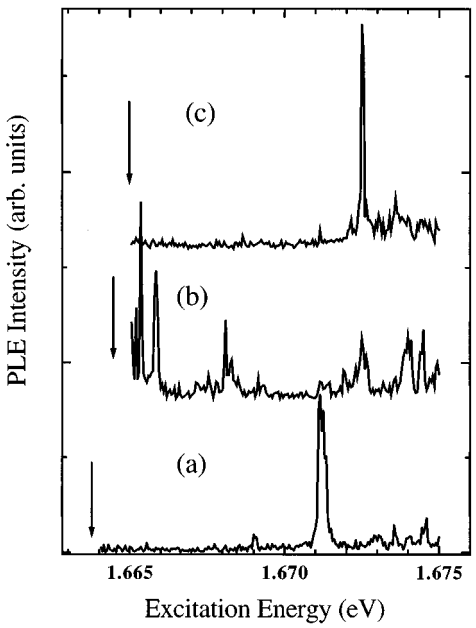

FIG. 5. Single-channel PLE spectra for the 28-Å QW in sample *B* measured through a 0.6-μm-diam aperture. The detector was set at three different energies: 1.66334 eV (a), 1.66407 eV (b), and 1.66448 eV (c).

The use of near-field spectroscopies allows the direct measurement of the homogeneous broadening of the excited states of the system as indicated by the Lorentzian shape of the sharp peaks of the spectra in Figs. 4 and 5. The emission peaks from these spectra have widths of 60 μeV approximately for the lowest-energy excited state and homogeneously increase with energy for further excited states. The FWHM for excited states go from 60 to 120 μeV. The error in these is mainly determined by the spectrometer resolution and it was estimated by using the spectral lines of a Ne lamp. Subtracting the Ne line broadening from the measured emission linewidths we obtained $\Gamma \sim 20$ μeV for the lowest-energy state, and values going from 20 to 80 μeV for higher excited states.

C. Electronic pictures

The dissimilarities found in the emission and absorption spectra of the two samples have their origin in two different electronic configurations as a result of different interface roughness profiles. In sample *A* the typical length scale of the growth islands is, generally, smaller than the exciton a_B. Small islands, i.e., those much smaller than a_B, can scatter excitonic states leading to modification of their energies and wave functions but they remain propagating states.[18] There are, however, a few islands large enough to confine the exciton center of mass in the plane of the well. In sample *A*, therefore, the excitonic state in a given region can be of either propagating or confined character. In the PL process, localized and extended excitons are optically created. Propagating excitons decay into confined states, which are at lower energies, during the thermalization step. Thus, the emission spectrum of this sample only shows the confined states. This explains why the absorption peaks are centered at higher energies and, also, why they are broader than the PL ones. In sample *B*, on the other hand, 2D islands are large ($\geqslant a_B$) thanks to the interruption of the growth at the interfaces. The lateral barriers of these islands are large enough to avoid tunneling through them during the lifetime of the confined states, as can be deduced from the PLE spectra of Fig. 5. With such a potential profile, sample *B* can be seen as an array of quantum boxes of different depths and shapes. The excitonic states in these wells are a solution of isolated quantum box potentials and have confined character if they are bound solutions of the potential or propagating character in the case of the continuum. The small values found for the Stokes shift between PL and PLE (Fig. 3) as well as the similar FWHM found for the transitions in both spectra indicate that, in contrast to what happens in sample *A*, in sample *B* almost all the states participate in the emission. The experimental results seem to suggest that the relaxation from higher- to lower-energy confined states in the interface islands occurs more slowly than the radiative recombination.

In good agreement with the electronic picture proposed for sample *B* are the near-field spectra of Figs. 4 and 5. In the PL spectrum of Fig. 4, the energy levels of the excitons confined in 2D islands depend on the island depth and radius, then the large number of sharp peaks correspond to the large diversity of lateral sizes. The existence of sharp transitions throughout the inhomogeneously broadened line proves that during the lifetime of the excitons these are confined in the 2D islands, which can be then seen as naturally formed quantum dots.[13] In a single-channel experiment, where the detection is restricted to one energy corresponding to a specific dot, we expect to see excitation transitions in this dot only for laser energies below the continuum edge. The high sensitivity found in sample *B*'s PLE spectra with respect to the detection energy confirms that slightly different detection energies correspond to different islands and the PLE spectrum obtained corresponds to a single dot that is optically isolated from the rest, in the sense that exciton relaxation between the dots does not occur.

As pointed out before, we expect that the total confinement of excitons found in sample *B* decelerates somehow the relaxation rate of higher- into lower-energy states. Relaxation processes between excited states separated by a few meV usually involve inelastic scattering by longitudinal acoustic (LA) phonons. The inelastic scattering (or relaxation) rate (τ_r^{-1}) and the spontaneous emission rate (τ_0^{-1}) give rise to the radiative broadening (Γ_{rad}) of the transition. Γ_{rad} can be associated to the lifetime of the state T_1 by $\Gamma_{\mathrm{rad}}=\hbar/T_1$. Elastic scattering processes contribute to the dephasing of the state and thus to its homogeneous broadening. This second contribution is known as collision broadening (Γ_{coll}) and, as with the radiative broadening, Γ_{coll} can be defined in terms of the dephasing time T_2' ($\Gamma_{\mathrm{coll}}=\hbar/T_2'$). In a two-level system the homogeneous broadening can be written in terms of these two components as

$$\Gamma=\Gamma_{\mathrm{rad}}+2\Gamma_{\mathrm{coll}}. \tag{5}$$

In 0D semiconductor structures, because of the total quantization of the energy, elastic scattering is forbidden[19] and the homogeneous broadening is entirely radiative. The linewidth measured by near-field PL for the lowest-energy excited state gives a very good approximation of the radiative recombination time of the state. Notice that the emission of phonons is forbidden for this state and, at low temperatures, the absorption of phonons is highly improbable. Typical broadenings measured in sample *B* were approximately 20 μeV, which correspond to lifetimes $T_1\approx\tau_0\approx 30$ ps. Higher excited-state broadenings measured by PLE monotonically increase with increasing energy. However, these states still show very small linewidths. Considering that the radiative recombination times of higher excited states are approximately equal to that for the first excited state, then relaxation times deduced from the experimental results are comparable with τ_0 ($\tau_r\geqslant 10$ ps). According to Bockelmann's calculations of quantum dot exciton radiative recombination times, the expected increase in τ_0 with increasing energy is attenuated as the confinement potential increases.[20] For the typical values of the lateral potential of sample *B*'s dots (~ 4 meV) τ_0 will increase below 5% for the excited state separated 10 meV from the lowest-energy state. It has been proved then that, although there is relaxation from higher- to lower-energy confined states (otherwise the intensity of the lowest-energy transition would have been very low), the relaxation time does not dominate the dynamics of 0D excitons and higher excited states also recombine radiatively. Our conclusions are coincident with previous results, which found that in 0D semiconductor systems the relaxation by LA phonons decreases strongly when the separation between energy levels is bigger than a certain value.[21,22]

D. Experimental apparatus

The experimental setup employed to measure the RRS of the two samples just described was the standard for a multichannel experiment: a titanium-doped sapphire laser was used as excitation source, the scattered light was dispersed by a 0.85-m focal length double monochromator and recorded by a charge-coupled device camera. Nevertheless two considerations have to be taken into account: (i) in order to minimize the nonresonant elastic scattering at the surface of the sample, the laser beam was incident at Brewster's angle [$\theta_B=\arctan(n_2/n_1)\approx 75°$] and detection was normal to the sample surface; (ii) due to the fact that the high coherence of the laser light could cause interference fringes via multiple reflection at the cryostat windows, interference modulation was prevented by focusing the laser beam onto a diffuser to reduce its spatial coherence before illuminating the sample. With the spectrometer fixed at the wavelength corresponding to the transition maximum, the laser was tuned across the exciton transition. The multichannel detection allowed the simultaneous measurement of the RRS and the PL spectra. The RRS and PL signals were carefully separated. By integrating the elastically scattered light for each excitation energy the RRS spectrum was obtained, and doing the same with the reemitted light for the whole hh transition it was possible to obtain the absorption spectrum, as pointed out at the beginning of this section.

IV. RRS VERSUS ABSORPTION

Important information about the origin of the RRS process can be obtained by comparing the RRS and the absorption spectrum[6] of a given transition. Figures 6(a) and 6(b) show RRS and PLE spectra for the 150-Å QW hh exciton of samples *A* and *B*, respectively, in terms of the laser detuning. While a measurable shift to lower energies of RRS with respect to absorption is found in sample *A*, its value is 150 ± 50 μeV, in sample *B* this redshift has decreased to 20 μeV, which is within the experimental error. Due to its similarities with the Stokes shift found between the emission and the absorption spectra in QW transitions, the red shift of the RRS with respect to the absorption has also been denoted as ''Stokes shift'' in the literature. From now on we will refer to it as Σ to avoid confusion, i.e., $\Sigma=E$(PLE peak)-E(RRS peak). The study of the magnitude of Σ was extended to different wells in both samples. As in the case of the PL-PLE spectra, it is found that while in sample *A* finite Σ is detectable and increases as the well width decreases, sample *B* shows an almost negligible shift. This behavior is reported in Figs. 6(c) and 6(d). These two figures show the RRS and the PLE spectra corresponding to the hh exciton transition of the

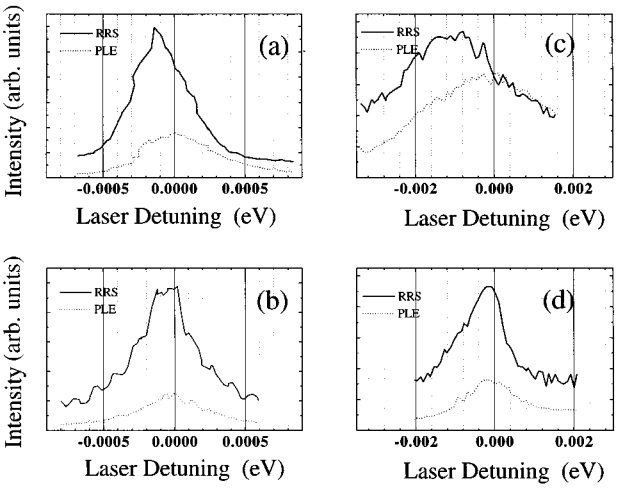

FIG. 6. RRS and absorption intensity profiles for the 150-Å hh exciton transitions in sample *A* (a) and sample *B* (b) and for the 60-Å hh transitions in samples *A* (c) and *B* (d). The *x* axis corresponds to the laser detuning ($\hbar\omega - E_0$).

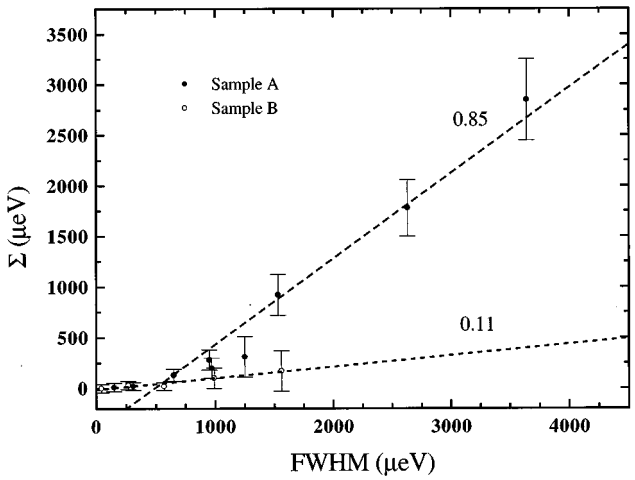

FIG. 7. Σ as a function of the FWHM of the PL peaks in the two different samples. The excitation power and the temperature were kept fixed at 10 μW/mm^2 and 8.5 K, respectively.

60-Å QW's in samples *A* and *B*, respectively. In this case Σ has increased to 0.92 meV in sample *A* while it is still lower than 0.2 meV in sample *B*.

To understand the origin of these different behaviors it is convenient to go back to the origin of the RRS process itself. Despite the analogy between PL and RRS, these two processes have completely different natures. PL is an incoherent process, which involves the relaxation of the real exciton population. RRS, on the other hand, comes from the coherent scattering of light as a consequence of the relaxation of wave-vector conservation in real solids, and for low excitation densities derives from exciton states and not from real exciton populations[8] (the Feynman diagrams of Fig. 1 involve virtual excitations of an initially unexcited system). Besides, while in PL it is the relaxation step that depopulates the propagating states before the emission, in RRS only localized states can participate in the process (as a first approximation; see Sec. II).

The measured Σ for the hh transitions of sample *A* can be explained in terms of the propagating and confined character of the ground state for different areas on the plane of the well for the single QW's of this sample. The peak of the RRS occurred at the lower-energy side of the absorption spectrum because confined exciton states give the main contribution to the scattering. The lack of Σ in sample *B*, on the other hand, cannot be interpreted as a sign of the lack of confined states. On the contrary, the dominant confined character of the states of sample *B* is responsible for the very low values of Σ in this sample. Σ does not depend on the confinement but on the electronic picture of the system. In Fig. 7 the measured Σ for the different transitions in the two samples is represented in terms of the FWHM of the emission, which must be proportional to the confinement energies of laterally bound states since here we do not eliminate the inhomogeneous broadening. Σ in both samples increases linearly with the emission linewidth. However, the rate of the increase with FWHM is very different from one sample to the other. Linear regression gives slopes of 0.85 and 0.11 for samples *A* and *B*, respectively, both very far from the 0.42 slope reported recently by Gurioli *et al.*[7], which they found to be sample independent.

A resonant enhancement of the elastic scattering was also observed for the bulk exciton transition of GaAs. Two features are remarkable in this case: the RRS signal is weaker than the one found at 2D transitions; and, more importantly, Σ is zero within the experimental error. The presence of defects in the perfect lattice breaks the periodicity of the potential and thus the conservation of wave vector is not required any longer. This is the mechanism responsible for RRS in bulk material and corresponds to diagrams including interaction with static defects in the diagrammatic picture of Fig. 1. The participation of static defects eliminates any constraint on the character of the intermediate states in this case, which is why $\Sigma \approx 0$. Because RRS by bulk excitonic states is a higher-order process and also because the density of impurities in the bulk is low in good samples, it is weaker than that measured on single QW's.

V. LINE-SHAPE ANALYSIS OF RRS

The presence or lack of an energy shift between RRS and PLE has been a recurrent topic in the scarce literature on resonant elastic scattering in 2D semiconductor systems.[1–7] However, no attention has been paid to the RRS intensity itself. Accepting that RRS in QW heterostructures is mainly produced by confined exciton states, a larger scattering enhancement would be expected in narrow wells where the confinement due to one monolayer fluctuations in the well width is stronger. In Fig. 8 the RRS scattering profiles for the hh exciton transitions of four wells in sample *A* are represented in terms of the energy detuning of the excitation energy with respect to the maximum of the RRS peak. The remarkable fast decay of the intensity maximum as the well width decreases is in contradiction with the initial assumptions. The same behavior is observed for sample *B*.

The understanding of the experimental results of Fig. 8 requires a careful analysis of the scattering process. In the calculations of the scattering efficiency of Belitsky *et al.*[8] the distribution of confined states was modeled by a completely

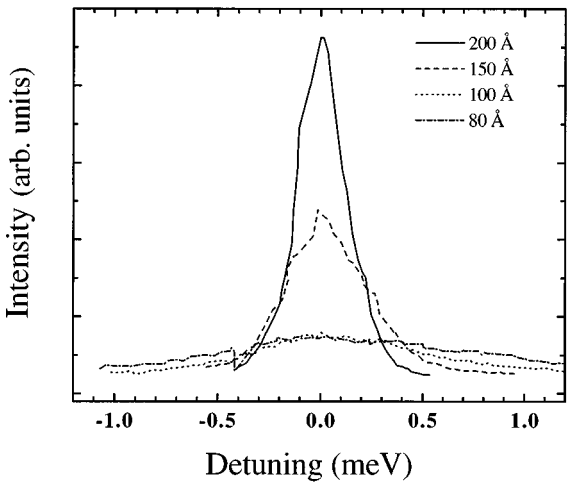

FIG. 8. RRS for different well width transitions as a function of the excitation detuning ($\hbar\omega - E_0$). The excitation power was fixed at 10 μW/mm^2 and $T = 8.5$ K.

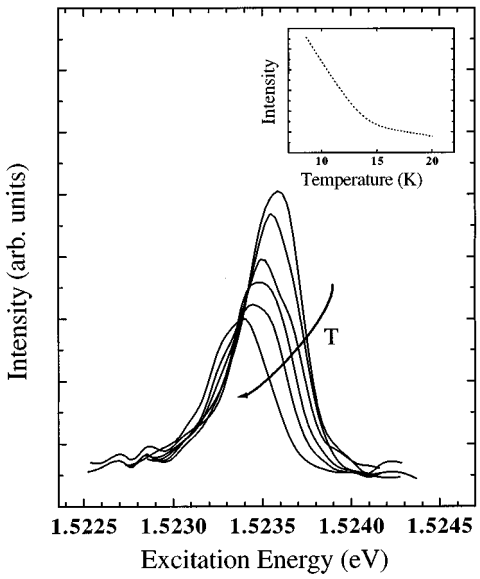

FIG. 9. RRS spectra for 200-Å QW for different temperatures. From right to left the peaks were measured at 8.3, 9.8, 13.2, 14.9, 17.1, and 19.9 K. The inset shows the temperature dependence of the RRS total intensity.

random spatial distribution and the differences in the confined energy due to the variation in the lateral size of the growth islands was reproduced by imposing Gaussian fluctuations in the state energy. The RRS efficiency then depends strongly on the ratio between the homogeneous and the inhomogeneous broadening Γ/Λ of the excitonic transitions (in that model Γ is the imaginary part of the state energy and Λ the Gaussian distribution width). As Γ/Λ decreases, the RRS peak becomes less intense and broader.[23] Transitions occurring in narrower wells present a bigger FWHM, or equivalently a bigger Λ, due to the stronger confinement potentials. Then, although in narrow wells the potential islands are deeper and the confinement is stronger, the scattering centers are distributed among a wider range of energies, causing weaker enhancement of the RRS.

Another factor that could affect the RRS intensity profiles of Fig. 8 is the angular dependence of the RRS process. According to Eq. (3) the in-plane transferred wave vector can be determined by the angle between the incident excitation beam and z. For incidence near to Brewster's angle and light wavelength in the red, Δk_{xy} is very small (it corresponds to $\Delta \ell_{xy} \sim 1\,\mu$m). The Fourier transform of the confined exciton wave function $\Phi(k_{xy})$ should have a peak at k_{xy} corresponding to confinement lengths of the order of a_B ($\sim$100 Å). This means that only the tail at low k_{xy} of $\Phi(k_{xy})$ is being probed in the experiment. As the well width decreases the potential from one-monolayer fluctuations increases and a_B decreases, thus the peak of $\Phi(k_{xy})$ moves towards larger k_{xy}, i.e., it moves away from the probed area, and the intensity of the measured signal drops.

For narrower wells (higher Λ) not only does the maximum of intensity decay for smaller well width (see the spectra corresponding to 100- and 80-Å QW's in Fig. 8) but also the broadening increases considerably. The comparison of the FWHM of the RRS, the PL, and the PLE spectra revealed that the RRS linewidth changes at the same rate as the PL broadening. And thus, while in sample *A* absorption peaks were wider than RRS transitions, especially for narrow wells, in sample *B* both widths are similar, which confirms that the main contribution to RRS in QW systems comes from confined excitonic states.

VI. TEMPERATURE DEPENDENCE OF RRS

Since confined excitons dominate the RRS in QW heterostructures, as shown in previous sections, we expect the RRS profile to be sensitive to changes in the temperature. The temperature dependence of the RRS spectrum was studied for several excitonic transitions in both samples. The measurements were made over a wide range of temperatures: from 1.4 to 40 K. For temperatures over 4.2 K a continuous-flow liquid-He cryostat was used. Temperatures from 1.4 to 4.2 K were achieved in a He bath cryostat. The sample temperature was measured by a four-point resistance measurement of a rhodium-iron sensor placed at the sample holder in the sample space of the cryostat. Figure 9 shows the evolution of the RRS spectrum at the hh exciton transition of a 200-Å QW when temperature varies from 8 to 20 K at a constant injection power. As the temperature is raised, apart from the shift to lower energies of the transition due to the diminution of the well and barrier band gaps,[24] the maximum of the peak decays as well as the total intensity of the process (see inset of Fig. 9).

Increasing the temperature can modify the homogeneous and the inhomogeneous broadenings of the excitonic transitions. The temperature dependence of the homogeneous broadening of excitons confined in interface roughness 2D islands has been recently studied by Gammon and co-workers.[13] It was found that up to 15 K the linewidth remains constant. Above this value it increases with a constant rate of 5 approximately μeV K^{-1}. The scattering with phonons increases for higher temperatures and so does the relaxation rate τ_r^{-1} contributing to the increase of the homogeneous broadening [Eq. (5)]. The inhomogeneous broadening also increases linearly with the temperature. The tem-

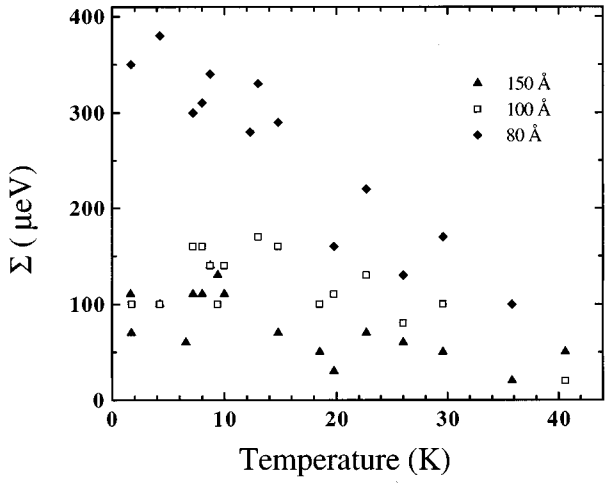

FIG. 10. Temperature dependence of Σ measured at the hh exciton transition corresponding to different well widths. The experimental errors of the points are of 60 μeV for the 150-Å QW and of 100 μeV for the 100- and 80-Å wells.

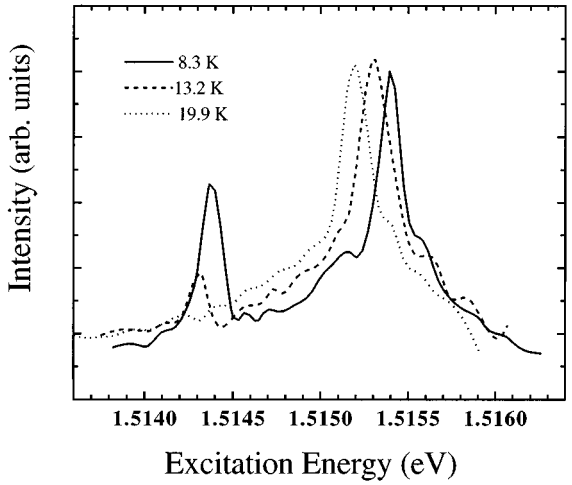

FIG. 11. Temperature evolution of the RRS spectra at the bulk exciton energy transitions.

perature coefficient varies from one author to another (values from 3.5 to 10 μeV K^{-1} can be found in the literature[25]) but in any case are comparable to the homogeneous broadening one. As temperature is raised the ratio Γ/Λ increases slightly. According to the Belitsky *et al.* model this effect contributes to an enhancement of the scattering efficiency, which is not seen in the experiment. Nevertheless the increase of Γ/Λ is very small, much smaller than the one that occurred with the variation of the well width, and no large effects can be expected from the variations in Γ/Λ due to changes in the temperature.

As temperature is raised, the increase in phonon mode occupancy makes it possible for other processes such as absorption of phonons to start to compete with the Rayleigh channel causing a decay in its efficiency. When the absorption of one or several phonons connects two real excitonic states the process is resonant and the photon emitted when the second exciton recombines contributes to the luminescence spectrum. If the final excitonic state has a propagating character the whole process can be seen as a thermal detrapping of excitons, which has already been studied by means of other techniques.[26] Because the probability of thermal detrapping is proportional to the population of phonons, described by the Bose-Einstein distribution $n_B = [\exp(\hbar\omega_p/k_BT)-1]^{-1}$, it increases with the temperature. As the temperature is raised the thermalization dominates and the RRS signal becomes weaker. Absorption of LA phonons is also the cause of the faster relaxation rate and the broader linewidths of the states. We point to the enhancement of the inelastic channels as the cause of the decay in the RRS intensity observed in the experiment (Fig. 9).

Thermal detrapping of excitons is also observed in the temperature evolution of Σ. Figure 10 shows the evolution of Σ with the temperature measured in the 150-, 100-, and 80-Å QW's of sample *A*. At low temperatures ($T \leqslant 10$ K) Σ remains constant or even increases slightly (see the evolution of the 100-Å QW). Above approximately 10 K, Σ of the transitions studied starts to decrease linearly. In terms of the detrapping picture presented above, as temperature starts to increase the shallower confined states can be promoted to delocalized states by the absorption of a phonon, and therefore these states do not contribute to the elastic scattering. In this first stage Σ may increase. Above a certain temperature all the localized states are accessible to thermal disorder and Σ starts to decrease.

Figure 11 reports the evolution of the RRS spectrum for the bulk exciton in GaAs with the temperature in the interval going from 8.3 to 19.9 K. At 8.3 K the RRS spectrum shows two peaks, the more intense corresponds to the fundamental exciton ($E_0 = 1.5153$ eV) and the other one corresponds to the exciton bound to a neutral impurity ($E' = 1.5143$ eV). In their evolution with the temperature, free and bound exciton states behave completely differently: while the intensity of the E' peak depends strongly on the temperature, E_0 remains constant as temperature increases. The free exciton probability of occupation does not change dramatically with the temperature in the range of temperatures of the experiment (up to 20 K), the bound exciton state, on the other hand, can be easily depopulated, i.e., ionized, as temperature increases (10 K $\equiv 0.862$ meV $\sim$ exciton bound energy).

VII. CONCLUSIONS

The optical investigations of two different samples presented in this paper have shown that the presence of a Stokes shift of the emitted signal with respect to the absorption is not a general feature of 2D systems. In contrast to the established idea of a Stokes shift increasing with the lateral confinement, we have given experimental evidence of the sensitivity of the Stokes shift to the interface roughness potential profile, which can be modified by the growth conditions. The same was observed for the energy shift between RRS and the absorption.

From the analysis of the intensity and line shape of the RRS spectra from exciton transitions in wells of different width, it has been concluded that the increase of confinement effects as the well width decreases and the concomitant increase of the inhomogeneous broadening of the transitions attenuates the enhancement of the elastic scattering and makes the RRS peaks broader as a consequence of the spread

in energy of the scattering centers.

Although the participation of propagating exciton states is not forbidden by the selection rules in QW systems, the main contribution to the RRS efficiency comes from states of confined character. The relaxation rate of these states is very sensitive to changes in the temperature. As temperature increases the inelastic channels involving absorption of thermally created phonons start to compete with the elastic scattering. This effect makes the RRS peaks become less intense. Thermally activated depopulation of confined states is also responsible for the decrease of Σ when the temperature increases.

The temperature evolution of the RRS for the bulk GaAs exciton was very different from that found for 2D transitions. The constant intensity of the RRS peak as temperature was raised proved that the nature of the process is different in this case: the intermediate states have propagating character and the scattering involves static defects in the crystal. The scattering efficiency in this case was proportional to the concentration of impurities, which does not depend on the temperature.

ACKNOWLEDGMENTS

This work was supported by EPSRC. We want to thank Dr. Dan Gammon who greatly assisted us in the initial stages of the work on the production of apertures and samples for the near-field PL. We are grateful to Dr. Fang Yang for so many useful discussions, and to Dr. Richard Harley (Southampton University) and Dr. David Richards for clarifying ideas and useful suggestions. Thanks are due to Dr. Andrés Cantarero for a critical reading of the manuscript.

[1] J. Hegarty, M. D. Sturge, C. Weisbuch, A. C. Gossard, and W. Wiegmann, Phys. Rev. Lett. **49**, 930 (1982).
[2] J. Hegarty, L. Goldner, and M. D. Sturge, Phys. Rev. B **30**, 7346 (1984).
[3] H. Stolz, *Time-Resolved Ligh Scattering from Excitons*, Springer Tracts in Modern Physics Vol. 130 (Springer, Berlin, 1994).
[4] H. Stolz, D. Schwarze, W. von der Osten, and G. Weimann, Superlattices Microstruct. **9**, 511 (1991).
[5] H. Stolz, D. Schwarze, W. von der Osten, and G. Weimann, Phys. Rev. B **47**, 9669 (1993).
[6] M. Gurioli, F. Bogani, A. Vinattieri, M. Colocci, V. I. Belitsky, A. Cantarero, and S. T. Pavlov, Solid State Commun. **97**, 389 (1996).
[7] M. Gurioli, F. Bogani, S. Ceccherini, A. Vinattieri, and M. Colocci, J. Opt. Soc. Am. B **13**, 1232 (1996).
[8] V. I. Belitsky, A. Cantarero, S. T. Pavlov, M. Gurioli, F. Bogani, A. Vinattieri, and M. Colocci, Phys. Rev. B **52**, 16 665 (1995).
[9] R. Zimmermann, Nuovo Cimento **17**, 1801 (1995).
[10] D. S. Citrin, Phys. Rev. B **54**, 14 572 (1996).
[11] D. S. Katzer, D. Gammon, and B. V. Shanabrook, J. Vac. Sci. Technol. B **10**, 800 (1992).
[12] K. Brunner, G. Abstreiter, G. Böhm, G. Tränkle, and G. Weimann, Appl. Phys. Lett. **64**, 3320 (1994).
[13] D. Gammon, E. S. Snow, B. V. Shanabrook, D. S. Katzer, and D. Park, Science **273**, 87 (1996).
[14] D. Gammon, E. S. Snow, and D. S. Katzer, Surf. Sci. **362**, 814 (1996).
[15] D. Gammon, E. S. Snow, B. V. Shanabrook, D. S. Katzer, and D. Park, Phys. Rev. Lett. **76**, 3005 (1996).
[16] H. Hillmer, A. Forchel, S. Hansmann, M. Morohashi, E. Lopez, H. P. Meier, K. Ploog, Phys. Rev. B **39**, 10 901 (1989).
[17] U. Jahn, S. H. Kwok, M. Ramsteiner, R. Hey, H. T. Grahn, and E. Runge, Phys. Rev. B **54**, 2733 (1996).
[18] G. Bastard, C. Delalande, M. H. Meynadier, P. M. Frijlink, and M. Voos, Phys. Rev. B **29**, 7042 (1984).
[19] T. Takagahara, J. Lumin. **44**, 347 (1989).
[20] U. Bockelmann, Phys. Rev. B **48**, 17 637 (1993).
[21] U. Bockelmann and G. Bastard, Phys. Rev. B **42**, 8947 (1990).
[22] K. Brunner, U. Bockelmann, G. Abstreiter, M. Walther, G. Böhm, G. Tränkle, and G. Weimann, Phys. Rev. Lett. **69**, 3216 (1992).
[23] See Figure 2 (a) of Ref. 8.
[24] S. Gopalan, P. Lautenschlager, and M. Cardona, Phys. Rev. B **35**, 5577 (1987).
[25] Johnson Lee, Emil S. Koteles, and M. O. Vassell, Phys. Rev. B **33**, 5512 (1986); Vivek Srinivas, John Hryniewicz, Yung Jui Chen, and Colin E. C. Wood, Phys. Rev. B **46**, 10 193 (1992); Vivek Srinivas, Yung Jui Chen, and Colin E. C. Wood, Solid State Commun. **89**, 611 (1994).
[26] C. Delalande, M. H. Meynadier, and M. Voos, Phys. Rev. B **31**, 2497 (1985).